



Changes in morphology and visual function over time in mouse models of retinal degeneration: an SD-OCT, histology, and electroretinography study

Tomoko Hasegawa¹ · Hanako O. Ikeda^{1,2} · Noriko Nakano¹ · Yuki Muraoka¹ ·
Tatsuaki Tsuruyama³ · Keiko Okamoto-Furuta³ · Haruyasu Kohda³ ·
Nagahisa Yoshimura¹

Received: 4 June 2015 / Accepted: 12 November 2015 / Published online: 5 January 2016
© Japanese Ophthalmological Society 2015

Abstract

Purpose To examine the long-term natural course of retinal degeneration in *rd10* and *rd12* mice using serial spectral-domain optical coherence tomography (SD-OCT), electroretinography/electroretinograms (ERGs), and histological analysis.

Methods Photoreceptor layer thickness and the ability to visualize photoreceptor ellipsoid zones were analyzed using SD-OCT images, and these images were compared with hematoxylin and eosin-stained sections and electron microscopy images. The a- and b-wave amplitudes of the ERGs were analyzed.

Results In *rd10* mice, the photoreceptor layer thickness rapidly decreased, and the photoreceptor ellipsoid zone was visible on SD-OCT images in 89 and 43 % of eyes of 21 and 33-day-old mice, respectively. In *rd12* mice, the photoreceptor layer gradually thinned, and the ellipsoid zone remained visible in 92 % of eyes at 19 months. Electron microscopy revealed that photoreceptor degeneration had occurred on the inner side of the outer nuclear layer in 21-day-old *rd10* and 7-month-old *rd12* mice, possibly due

to autophagy mechanisms. Scotopic ERGs of *rd10* mice showed a diminished response at 21 days; at 33 days, no response was detectable. In *rd12* mice, scotopic ERGs were undetectable at 28 days (stimulus intensity 3.0 cds/m²). Photopic ERGs were nearly undetectable in 28-day-old *rd10* mice, but a small b-wave was still recordable in 13-month-old *rd12* mice.

Conclusions Our results demonstrate that visual function deteriorated with photoreceptor degeneration within 1 month in *rd10* mice. In *rd12* mice, however, the process of visual function deterioration and photoreceptor degeneration was still in progress at 13 months of age.

Keywords *rd10* · *rd12* · Retinal degeneration · Longitudinal study · Spectral-domain optical coherence tomography

Introduction

Retinitis pigmentosa is the most common type of retinal degeneration, with approximately 1.5 million affected people around the world and an incidence ranging from 1 in 3000 to 1 in 5000 people [1]. To date, no established therapies exist. Consequently, scientists throughout the world are working to develop effective potential therapies, including regenerative medicine [2], gene therapy [3, 4], and neurotrophic factor therapy [5–7].

Although more than 100 genes are reported to be associated with the retinal degeneration observed in patients with retinitis pigmentosa [8], it is a very heterogeneous condition, and most genes are responsible for only a small proportion of the cases [9]. The causative genes for retinitis pigmentosa and Usher syndrome were studied in a Japanese population by Oishi et al. [10]. These authors reported

Electronic supplementary material The online version of this article (doi:10.1007/s10384-015-0422-0) contains supplementary material, which is available to authorized users.

✉ Hanako O. Ikeda
hanakoi@kuhp.kyoto-u.ac.jp

¹ Department of Ophthalmology and Visual Sciences, Kyoto University Graduate School of Medicine, 54 Kawahara-cho Shogoin, Sakyo-ku, Kyoto 606-8507, Japan

² Institute for Advancement of Clinical and Translational Science, Kyoto University Hospital, Kyoto, Japan

³ Center for Anatomical Studies, Kyoto University Graduate School of Medicine, Kyoto, Japan

that although *EYS* and *USH2A* were the two most common causative genes, accounting for 28.9 and 9.1 % of causative genes, respectively, genes involved in the visual cascade, such as *RHO* and *PDE6B* (rod cGMP phosphodiesterase gene) accounted for a relatively high percentage of causative genes (5.8 and 5.0 %, respectively) [10]. The *PDE6*-encoded proteins play a role in cGMP hydrolysis and photoreceptor hyperpolarization. The *RPE65* gene (encoding retinal pigment epithelium 65 protein) is involved in the conversion of all-*trans* retinol to 11-*cis* retinal during photoreceptor phototransduction and visual pigment regeneration. In addition to be associated with retinitis pigmentosa, mutated forms of *RPE65* have been found in some cases of Leber congenital amaurosis (LCA) [11]. Although Oishi et al. [10] found that *RPE65* accounted for only a small proportion of causative genes, this gene has been the focus of much attention, and clinical trials with patients bearing this gene mutation are ongoing [12–14].

Among spontaneous mouse models of retinal degeneration, *rd1* and *rd10* mice have mutations in the *Pde6b* gene, and *rd12* mice have mutations in the *Rpe65* gene. *rd10* mice have a missense mutation in the *Pde6b* gene on exon 13 [15]. *rd10* has been widely used as a model system for the study of retinal degeneration because the onset and progression of retinal degeneration is milder than in the *rd1* mouse model, which has a nonsense mutation in the *Pde6b* gene [16]. The *rd12* mouse has a nonsense mutation in the *Rpe65* gene on exon 3 [17].

In order to understand disease progression mechanisms and to develop new treatments, it is essential to observe the precise natural course of hereditary retinal degeneration in animal models. Several studies have examined this in the mouse model using a variety of methods, including electroretinography (ERG), ophthalmoscopy, fundus photography, and histology [15, 17–19]. The relatively recent development of optical coherence tomography (OCT) has greatly increased our ability to assess retinal diseases in clinical and experimental settings [20, 21]. Spectral domain OCT (SD-OCT) has enabled researchers to obtain clearer, more detailed retinal images in vivo [22] and has been used in experimental rodent models [23–28]. Retinal thickness measurements by SD-OCT correlate well with histological measurements [23, 24, 26–28]. Huber et al. [23] and Kim et al. [24] performed SD-OCT on mice with various retinal degenerations to monitor longitudinal retinal degeneration. Wang et al. [28] report a good correlation between SD-OCT images and ERGs in *Rho*^{-/-} mice. Pang et al. [25] and Pennesi et al. [26] assessed *rd10* mice with SD-OCT, ERG, and histology. However, only a few studies have used SD-OCT to examine the long-term histological and functional courses of *rd10* or *rd12* mice.

In the study reported here, we assessed and compared the long-term longitudinal course of *rd10* and *rd12* mice

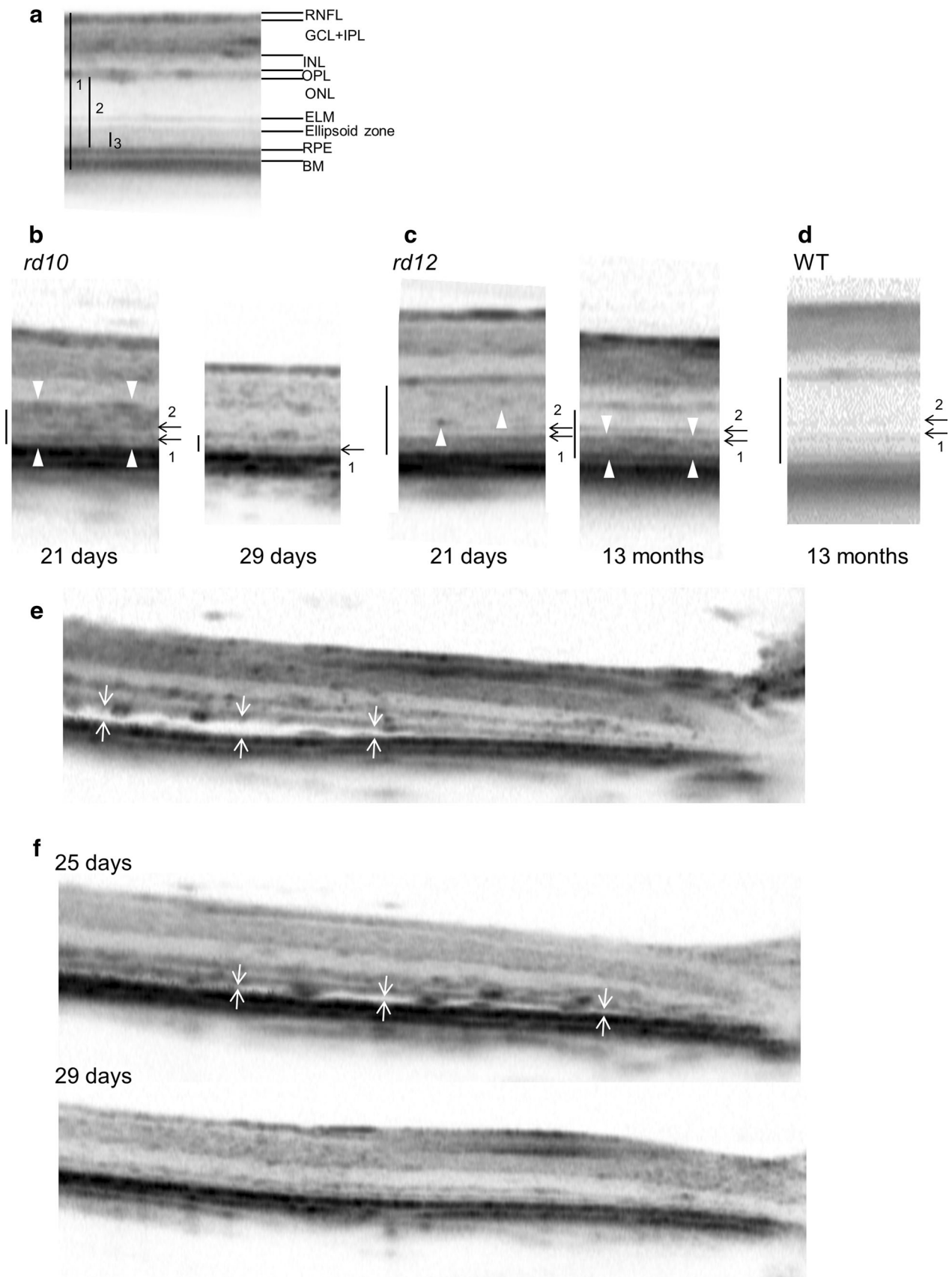
Fig. 1 Spectral domain optical coherence tomography (SD-OCT) images of *rd10*, *rd12*, and wild-type (WT) mice. **a** An SD-OCT image of a WT mouse showing the retinal nerve fiber layer (RNFL), the ganglion cell layer (GCL), the inner plexiform layer (IPL), the inner nuclear layer (INL), the outer plexiform layer (OPL), the outer nuclear layer (ONL), the external limiting membrane (ELM), the photoreceptor ellipsoid zone (Ellipsoid zone), and the retinal pigment epithelium (RPE). Vertical black bars: 1 Total retinal thickness, 2 photoreceptor layer thickness (sum of ONL, myoid zone, ellipsoid zone, and photoreceptor outer segment thickness), 3 photoreceptor outer segment (OS) layer. **b** The SD-OCT images from 21- and 29-day-old *rd10* mice. At 21 days (left image), the photoreceptor ellipsoid zone (black arrow 1) was visible and the ELM (black arrow 2) was partially visible. Hyper-reflections were seen from the ONL to the OS layer (white arrowheads). At 29 days (right image), the ONL was not hyper-reflective and the OS layer was diminished. The ellipsoid zone was visible (black arrow 1), but the ELM was not. Black bar indicates the thickness of the photoreceptor layer. **c** The SD-OCT images of 21-day- and 13-month-old *rd12* mice. At 21 days (left image), the ellipsoid zone (black arrow 1) was visible, but the ELM (black arrow 2) was partially visible. The ONL was weakly and focally hyper-reflective (white arrowheads). At 13 months (right image), the ellipsoid zone (black arrow 1) was visible, but the ELM (black arrow 2) was partially visible. The OS layer was hyper-reflective (white arrowheads). Black bars indicate the thickness of the photoreceptor layer. **d** An SD-OCT image of a 13-month-old WT mouse. The ellipsoid zone (black arrow 1) and ELM (black arrow 2) were visible and no hyper-reflective layer was seen. Black bar indicates the thickness of the photoreceptor layer. **e** An SD-OCT image of a 25-day-old *rd10* mouse with serous retinal detachment (white arrows). **f** An SD-OCT image of 25-day-old *rd10* mouse with serous retinal detachment (white arrows); the detachment was no longer present at 29 days. For a description of the *rd10* and *rd12* mutations see text of Section Introduction

retinas by examining both retinal morphology and function. Electron microscopy, hematoxylin and eosin (HE) section staining, SD-OCT, and ERG were performed.

Materials and methods

Experimental animals

This study was conducted in accordance with the Association for Research in Vision and Ophthalmology Statement for the Use of Animals in Ophthalmic and Vision Research. All protocols were approved by the Institutional Review Board of Kyoto University Graduate School of Medicine (MedKyo13221, 14213). All *rd10* mice and *rd12* mice were obtained from the Jackson Laboratory (Bar Harbor, ME). All mice were maintained in a 14-h light/10-h dark cycle and were fed ad libitum. Before image or ERG acquisition, mice were anesthetized with an intramuscular injection of a ketamine (70 mg/kg)/xylazine (14 mg/kg) mixture. Pupils were dilated to a diameter of approximately 2 mm with tropicamide (1.67 mg/mL) and phenylephrine (1.67 mg/mL) eye drops. To prevent anesthesia-induced



dry eyes, a hydroxyethyl cellulose eye solution (Scopisol; Senju Pharmaceutical, Osaka, Japan) was applied to the corneas during examination and eye ointment containing 0.3 % ofloxacin were applied to the corneas after the examination.

OCT image acquisition

Fundus images were obtained using a custom-made speckle noise-reduced SD-OCT, with the eye-tracking function based on Spectralis® HRA + OCT (Multiline OCT; Heidelberg Engineering, Heidelberg, Germany). Before imaging, all eyes were fitted with a polymethyl methacrylate contact lens that is optimal for the mouse eye (Nichicon, Osaka, Japan) to prevent anesthesia-induced cataract progression and drying up of the cornea, as previously reported [29]. With the PMMA contact lens placed on the mouse cornea, the total focal length was 2.00 mm (in air), which is scaled at 16.447 mm (in air) in the human eye. We multiplied the values (millimeters) of the Spectralis by a factor of $2.00/16.447 = 0.122$ to obtain the lateral values in mouse eye, as previously reported [29]. A 25-diopter adaptor lens was placed on the objective lens of the Multiline OCT to focus onto the mouse retina. The scan rate of the SD-OCT is 47,000 A-scans per second, with an axial resolution of approximately 7 μm . A vertical B-scan through the optic disc was obtained, along with 19 vertical B-scans evenly spaced over a $30^\circ \times 15^\circ$ area through the optic nerve head for volume mapping [30]. One hundred individual B-scans (manufacturer-set maximum) were averaged to obtain the final vertical B-scan, and 50 individual B-scans were averaged for each of the 19 vertical B-scans used in volume mapping around the optic nerve head. The *rd10* mice were examined when they were between 21 and 52 days old, and the *rd12* mice were examined when they were between 21 days and 19 months old. Wild-type (WT) mice were also examined for comparison.

Analyses of OCT images

The photoreceptor ellipsoid zone, commonly referred to as the inner/outer segment junction, and the external limiting membrane (ELM) lines on SD-OCT images were characterized as visible, partially visible, or not visible. Some *rd10* mice developed a serous retinal detachment. These eyes were excluded from SD-OCT assessments of retinal thickness when the retinal detachment was detected, but they were not excluded from assessments of the ellipsoid zone or ELM in order to avoid selection bias because a relatively large number of eyes developed retinal detachment.

We assessed total retinal thickness, evaluated as the distance between the inner limiting membrane and the outer side of the Bruch's membrane (black bar "1" in Fig. 1a). The thickness of the photoreceptor layer was evaluated as the sum of outer nuclear layer thickness and photoreceptor inner/outer segment layer thickness (black bar "2" in Fig. 1a). The vitreoretinal interface, outer plexiform layer/outer nuclear layer (ONL), retinal pigment epithelium (RPE) anterior border, and Bruch's membrane posterior border were manually determined. The built-in software of the Spectralis® HRA + OCT system was then used to create a volume map around the optic nerve head which in turn was used to assess total retinal thickness within 366 μm of the optic nerve head in all directions (circular area). The circular area within 122 μm of the optic nerve head was excluded from the analyses. Measured values of the upper, lower, right, and left regions were averaged [Electronic Supplementary Material (ESM) Fig. S1a]. The thickness of the photoreceptor layer was measured 244 μm above and below the center of the optic nerve head using a single vertical scan. These two measurements were then averaged to obtain the final photoreceptor layer thickness measurement (ESM Fig. S1b).

Electroretinogram recordings

Following overnight dark adaptation of the mice, scotopic ERGs were recorded using a gold-loop corneal electrode with a light-emitting diode (Mayo Corp., Inazawa, Japan). A reference electrode was placed in the mouth of the mouse, and a ground electrode was placed in the anus. Stimuli were produced with a light-emitting diode stimulator (Mayo Corp.). The ERG response signals were amplified (PowerLab 2/25; AD instruments, Castle Hill, NSW, Australia). The stimulus intensity was 3.0 and 30.0 cd/m^2 , and up to four responses (stimulus interval ≥ 60 s) were averaged to obtain the final scotopic ERG waveform. Scotopic ERGs were recorded from *rd10* mice aged between 21 and 33 days and from *rd12* and WT mice at age 28 days. Photopic ERGs were also recorded, with a stimulus intensity of 3.0, 10.0, and 30.0 cd/m^2 , respectively, under a background illumination of 30 cd/m^2 [31]. The final photopic ERG waveform was the average of 30–50 responses (stimulus interval 1.0 s). Photopic ERGs were recorded in *rd10* mice aged between 21 and 49 days and in *rd12* and WT mice aged between 1 and 13 months. The a- and b-wave amplitudes were analyzed using Chart & Scope software (AD instruments).

Histological retinal evaluations

Eyeballs were enucleated immediately after the animals were euthanized with a pentobarbital overdose. A dye was

placed on the edge of the superior conjunctiva to mark the superior portion of the retina, following which the eyes were fixed in 4 % paraformaldehyde for 24 h at 4 °C and embedded in paraffin. The paraffin-embedded tissue was then cut into 6- μ m-thick sections through the dye mark and the optic nerve insertion point. Sections that included the center of the optic nerve head were stained with HE and photographed under an optical microscope (BZ-9000; Keyence, Tokyo, Japan). The HE-stained retinal sections used in analyses were obtained from 21- to 56-day-old *rd10* mice and from 13- to 19-month-old *rd12* mice.

Electron microscopy

Electron microscopy images of the retina were obtained from a 21-day-old *rd10* mouse, a 7-month-old *rd12* mouse, and a 19-month-old *rd12* mouse. After perfusion fixation

with 4.0 % paraformaldehyde, the enucleated eyes were immediately postfixed overnight in a mixture of 2.5 % glutaraldehyde and 10 % formaldehyde. Further fixation was done by immersing the tissue in 1 % osmium tetroxide for 90 min. The retinas were then dehydrated [with a graded series of ethanol (50–100 %) baths], cleared in propylene oxide, and embedded in epoxy resin. Ultrathin sections were cut with an ultramicrotome and stained with uranyl acetate and lead citrate. Stained sections were then examined with transmission electron microscopy (model H-7650; Hitachi Co., Tokyo, Japan).

Statistical analyses

Data are presented as mean \pm standard deviation (SD). One-way analysis of variance repeated measures and the Bonferroni post hoc test were used to compare parameters.

Table 1 Ellipsoid zones and external limiting membrane lines in *rd10* mice

Ellipsoid zones/external limiting membrane lines	Age (days)				
	21	25	29	33	52
<i>n</i> (eyes/mice)	27/14	26/13	14/7	14/7	13/7
Ellipsoid zone					
Visible	12 (44 %)	5 (19 %)	3 (21 %)	2 (14 %)	0
Partially visible	12 (44 %)	17 (65 %)	7 (50 %)	4 (29 %)	0
Not visible	3 (11 %)	4 (15 %)	4 (29 %)	8 (57 %)	13 (100 %)
External limiting membrane					
Visible	9 (33 %)	0	0	0	0
Partially visible	2 (7 %)	0	0	0	0
Not visible	16 (59 %)	26 (100 %)	14 (100 %)	14 (100 %)	13 (100 %)
Retinal detachment	0	8 (31 %)	1 (7 %)	1 (7 %)	12 (92 %)

Data are presented as the number of eyes, with the percentage in parenthesis

Table 2 Ellipsoid zone and external limiting membrane lines in *rd12* mice

Ellipsoid zones/external limiting membrane lines	Age					
	21 days	1 month	2 months	4 months	13 months	19 months
<i>n</i> (eyes/mice)	18/10	12/6	12/6	12/6	16/8	13/7
Ellipsoid zone						
Visible	17 (94 %)	12 (100 %)	12 (100 %)	12 (100 %)	9 (56 %)	1 (8 %)
Partially visible	1 (6 %)	0	0	0	5 (31 %)	11 (85 %)
Not visible	0	0	0	0	2 (13 %)	1 (8 %)
External limiting membrane						
Visible	2 (11 %)	0	5 (42 %)	1 (8 %)	0	1 (8 %)
Partially visible	16 (89 %)	11 (92 %)	7 (58 %)	10 (83 %)	12 (75 %)	6 (46 %)
Not visible	0	1 (8 %)	0	1 (8 %)	4 (25 %)	6 (46 %)
Retinal detachment	0	0	0	0	0	0

Data are presented as the number of eyes, with the percentage in parenthesis

The unpaired *t* test was used to compare parameters between *rd10*, *rd12*, and WT mice. Statistical significance was defined as $P < 0.05$.

Results

Each retinal layer was clearly observed on SD-OCT images of WT mice retinas (Fig. 1a). The photoreceptor ellipsoid zone, also known as the inner/outer segment (IS/OS) junction line, is known to be correlate with visual function [32, 33] and was visible in all eyes throughout the observation period (ESM Table S1). The ELM line, which has also been correlated with good visual function [34], also remained visible or partially visible in WT mice at all ages (ESM Table S1). In 21-day-old *rd10* mice, the ellipsoid zone was visible in 44 % eyes, partially visible in 44 % eyes, and not visible in 11 % eyes. The percentage of the

Fig. 3 Hematoxylin and eosin (HE)-stained retinal sections from *rd10*, *rd12*, and WT mice. **a** HE-stained sections of *rd10* mice at 21, 25, 29, 33, and 56 days of age. A stained section from a 56-day-old WT mouse is shown for comparison. In *rd10* mice, a progressive thinning of the outer nuclear layer (ONL) thinning is evident, but the inner retina is preserved. Outer segments (OS) are disorganized at 21 days and have almost disappeared at 29 days. A retinal detachment is seen at 56 days. **b** The HE-stained sections of *rd12* mice at 13 and 19 months. A stained section from a 13-month-old WT mouse is shown for comparison. In *rd12* mice, ONL thinning and OS disorganization is evident. Scale bar: 50 μm

eyes with a visible ellipsoid zone decreased with age. At 33 days of age, the zone was visible in only 14 % eyes. At 21 days of age, the ELM was visible or partially visible in 41 % eyes, but just 4 days later (25 days), the line was not visible in any eye examined (Table 1). In contrast, the ellipsoid zone was visible in all 4-month-old *rd12* mice, remaining visible or partially visible in 92 % eyes at

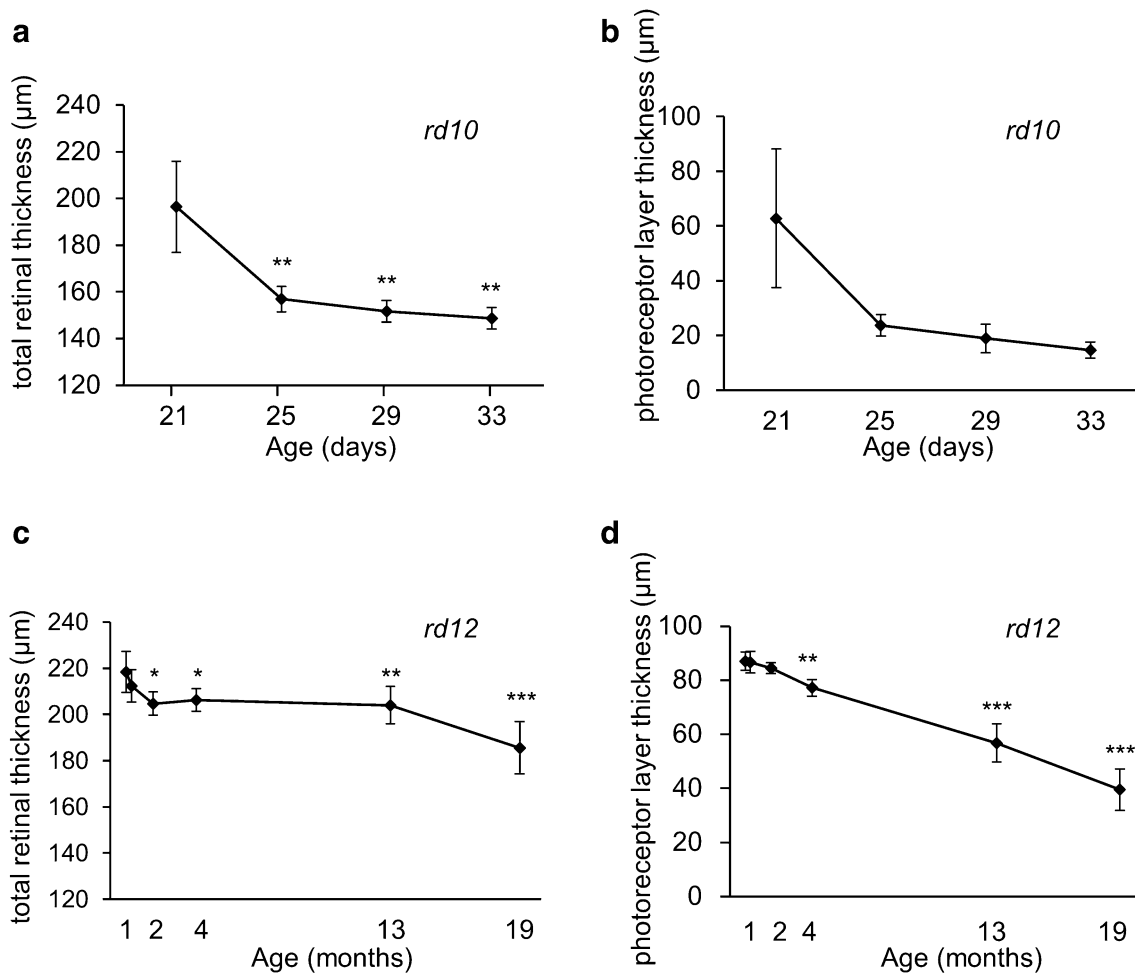
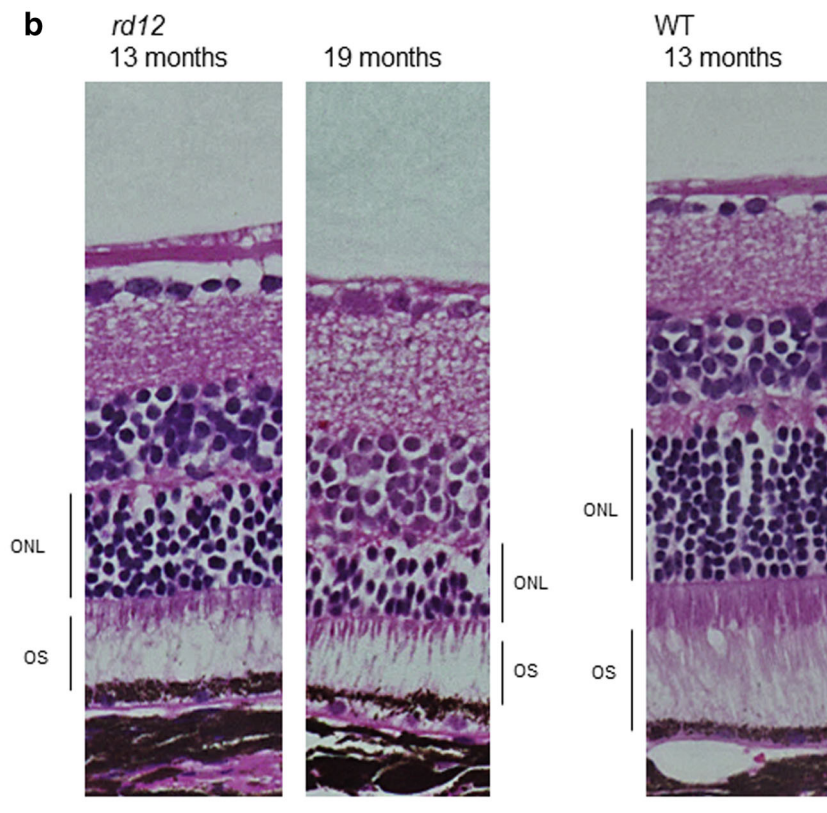
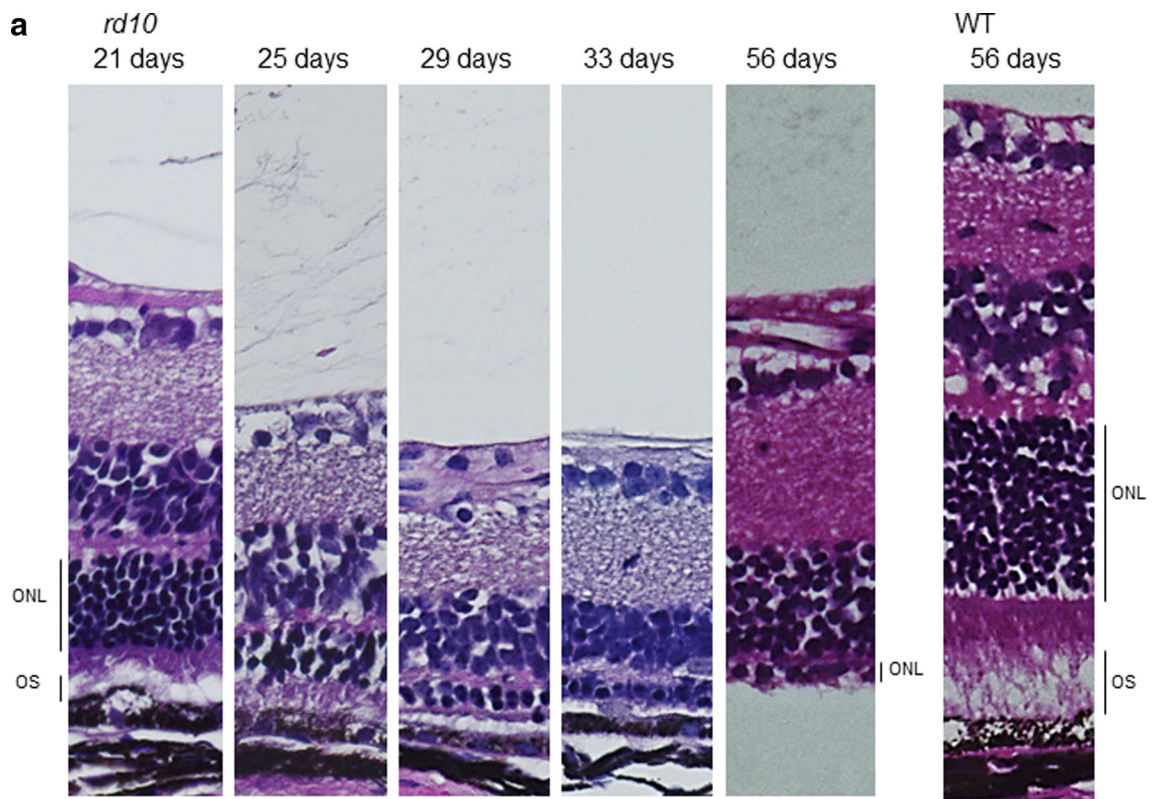


Fig. 2 Total and photoreceptor layer thickness in *rd10* and *rd12* mice. **a**, **b** Total retinal (**a**) and photoreceptor layer thickness (**b**) of *rd10* mice rapidly decreased during the observational period. **c**, **d** Total retinal (**c**) and photoreceptor layer thickness (**d**) of *rd12* mice

slowly decreased during the observational period. * $P < 0.05$; ** $P < 0.01$; *** $P < 0.001$ vs. thickness at 21 days, Bonferroni post hoc test



19 months. The ELM line was visible or partially visible in all eyes at 21 days and remained visible or partially visible in 54 % eyes at 19 months (Table 2).

Analysis of the SD-OCT images revealed that 81 % of eyes of 21-day-old *rd10* mice had a higher reflectivity in the ONL and OS layer than the eyes of WT mice (Fig. 1b, d). In contrast, 67 % eyes of 21-day-old *rd12* mice had a hyper-reflective ONL. Additionally, the hyper-reflectivity was only found in part of the ONL, and it was weaker than that seen in *rd10* mice (Fig. 1b, c). In later disease stages in *rd10* mice, the ONL hyper-reflection was no longer visible, and the layer corresponding to the photoreceptor OS was almost undetectable (Fig. 1b). In *rd12* mice, the ONL hyper-reflection remained visible until 4 months of age. In some cases, the photoreceptor OS hyper-reflection was also observed at later stages, with 33 % of eyes, 25 % of eyes, and 15 % of eyes having this feature at 4, 13, and 19 months, respectively (Fig. 1c).

Interestingly, a shallow serous retinal detachment was observed in eight of 26 eyes (31 %) of 25-day-old *rd10* mice (Fig. 1e, f; Table 1). Of these eight eyes with a retinal detachment, three were continuously examined; the retinal detachment resolved spontaneously in all eyes within 4 days, but the OS layer was diminished (Fig. 1f). At 52 days of age, retinal detachment was again observed in 92 % of eyes. The SD-OCT images obtained from eyes that had a retinal detachment were excluded from the retinal thickness assessments. No retinal detachments were observed between 21 days and 19 months in *rd12* mice (Table 2).

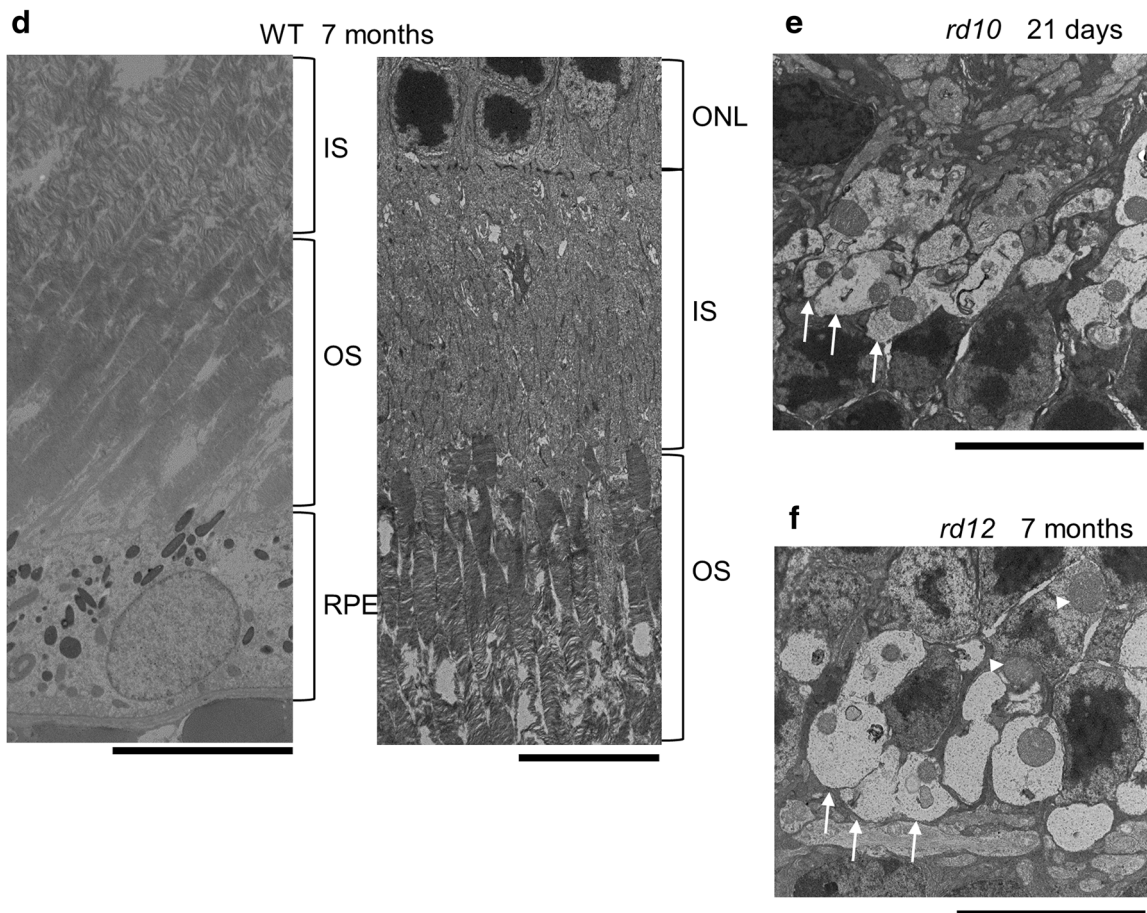
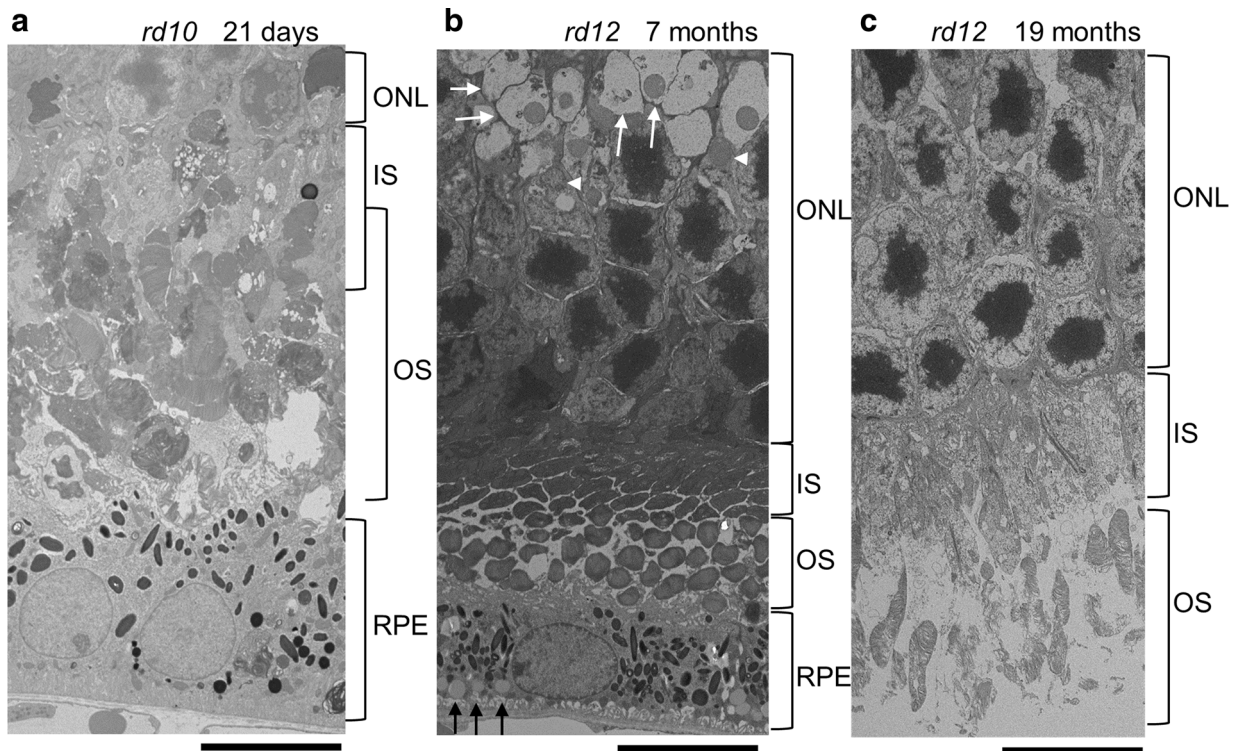
Total retinal thickness (bar “1” in Fig. 1a) and photoreceptor layer thickness (bar “2” in Fig. 1a) were also assessed (ESM Fig. S1a, b). At 21 days in *rd10* mice, total retinal thickness measured 196.4 ± 19.5 and photoreceptor layer thickness measured 62.8 ± 25.3 μm . These values rapidly decreased over time and were 148.7 ± 4.6 and 14.7 ± 2.9 μm , respectively, at 33 days (Fig. 2a, b). In *rd12* mice, total retinal thickness and photoreceptor thickness gradually decreased over time (Fig. 2c, d), with measurements of total retinal thickness and photoreceptor thickness of 218.3 ± 8.9 and 87.0 ± 3.4 μm at 21 days, 206.3 ± 4.8 and 77.2 ± 3.0 μm at 4 months, and 204.0 ± 8.0 and 56.8 ± 7.1 μm at 13 months, respectively. The total thickness of both the retina and photoreceptor kept decreasing from 13 to 19 months (185.6 ± 11.4 and 39.5 ± 7.6 μm , respectively, at 19 months; $P = 0.022$ and $P < 0.0001$ compared to 13 months). In WT mice, retinal thickness did not decrease between 21 days and 13 months.

To confirm our SD-OCT findings, we also performed histological analyses. The HE-stained sections of *rd10* mice retinas showed a progressive decrease in photoreceptor nuclei as well as ONL thinning (Fig. 3a). In the

Fig. 4 Electron microscopy images of *rd10*, *rd12*, and WT retinas. **a** Image of a 21-day-old *rd10* mouse retina. Degeneration and disorganization were observed in the outer nuclear layer (ONL) and outer segment (OS) layer. **b, c** Images of a 7-month-old mouse *rd12* mouse retina (**b**) and a 19-month-old *rd12* mouse retina (**c**). Lipid-like droplets are visible in the retinal pigment epithelium of the 7-month-old *rd12* mouse retinas (black arrows in **b**); outer segment disorganization is evident in a 19-month-old *rd12* mouse retina (**c**). **d** Images of WT mouse retina. **e, f** Magnified images of the ONL in 21-day-old *rd10* (**e**) and 7-month-old (**f**) *rd12* mouse retinas. Intracellular vacuoles are seen in photoreceptor cells at the innermost ONL in 21-day-old *rd10* (white arrows in **e**) and 7-month-old *rd12* mice retinas (white arrows in **b, f**). In addition to vacuoles, many intracellular circular organelles (white arrow heads in **b, f**) other than the nucleus were observed in cell bodies of the ONL. IS Inner segment, RPE retinal pigment epithelium. Scale bars (**a–f**): 10 μm

retina of 33-day-old *rd10* mice, only one to two rows of photoreceptor nuclei were observed. The OS layer had already thinned and was disorganized at 21 days. By 29 days, it had almost disappeared. At 56 days, a retinal detachment was seen, as observed on SD-OCT images. In comparison to the retinas of WT mice, the HE-stained sections of *rd12* mice retinas showed ONL thinning and OS disorganization at 13 months (Fig. 3b). By 19 months, there was further thinning of the ONL in *rd12* mice, but five to six rows of photoreceptor nuclei remained present at this time-point. Electron microscopy images of 21-day-old *rd10* mice eyes showed ONL and OS degeneration and disorganization (Fig. 4a) compared to WT mice retinas (Fig. 4d). In 7-month-old *rd12* mice, the ONL, IS, and OS were only slightly disorganized, while in 19-month-old *rd12* mice, the OSs were severely disorganized (Fig. 4b, c). Lipid-like droplets appeared in the RPE cytoplasm of 7-month-old *rd12* mice retinas (Fig. 4b; black arrows). In 7-month-old *rd12* and 21-day-old *rd10* mice, photoreceptor cells in the ONL had intracellular vacuoles surrounded by membranes (Fig. 4b, e, f; white arrows). Changes presented at the innermost ONL. In addition, many intracellular circular organelles (white arrowheads) other than the nucleus were observed in cell bodies of the ONL; this was rarely observed in WT retinas.

The scotopic ERG was performed to examine retinal function. In 21-day-old *rd10* mice, a-wave (reflects rod photoreceptor response [35]), b-wave (derived from bipolar cells [36]), and oscillatory potentials (derived from amacrine cells [37]) were all present (a-wave amplitude 175.6 ± 130.6 μV ; b-wave amplitude 323.8 ± 229.3 μV ; stimulus intensity 3.0 cds/m^2). However, compared to WT mice ERGs [a-wave amplitude 255.1 ± 100.5 μV ($P = 0.036$); b-wave amplitude 536.9 ± 194.3 μV ($P = 0.002$); stimulus intensity 3.0 cds/m^2], the amplitudes of these ERG components of 21-day-old *rd10* mice were smaller, and the wave peaks were delayed (Fig. 5a). The



a-wave was almost non-recordable in 25-day-old *rd10* mice (Fig. 5a). The b-wave amplitude rapidly decreased as the photoreceptor layer thinned and, at 33 days, the b-wave was almost undetectable (Figs. 2a, b, 5a, c). In 28-day-old *rd12* mice, the photoreceptor layer thickness was near normal, but the scotopic ERG was not recordable at a stimulus intensity of 3.0 cds/m²; compared to WT mice (a-wave amplitude 376.2 ± 128.6 μV; b-wave amplitude 686.8 ± 182.6 μV), only a small and delayed b-wave (amplitude 80.3 ± 49.0 μV; $P < 0.001$) was detectable at a stimulus intensity of 30.0 cds/m² (Figs. 2c, d, 5b).

Photopic ERGs were also recorded to examine photoreceptor function in the light-adapted conditions. The b-wave amplitude in WT mice slightly diminished with age (Fig. 6c). In 21-day-old *rd10* mice, the photopic ERG b-wave was small (b-wave amplitude 20.8 ± 11.6, 38.0 ± 20.9, and 101.1 ± 55.9 μV at stimulus intensities of 3.0, 10.0, and 30.0 cds/m², respectively), but oscillatory potentials were present. By day 28, the b-wave was diminished and was no longer recordable in many eyes (Fig. 6a, d; $P = 0.279$, $P < 0.0001$, and $P = 0.001$ vs. b-wave day 21 at stimulus intensities of 3.0, 10.0, and 30.0 cds/m², respectively). In *rd12* mice, the b-wave was present at 1 month of age (b-wave amplitude 8.6 ± 2.9, 17.9 ± 13.1, and 88.2 ± 57.8 μV at stimulus intensities of 3.0, 10.0, and 30.0 cds/m², respectively), following which its amplitude rapidly decreased until 3 months of age. Although small, the b-wave remained detectable at 13 months of age (Fig. 6b, e; b-wave amplitude 9.4 ± 4.5 and 25.4 ± 19.1 μV at stimulus intensities of 10.0 and 30.0 cds/m², respectively).

Discussion

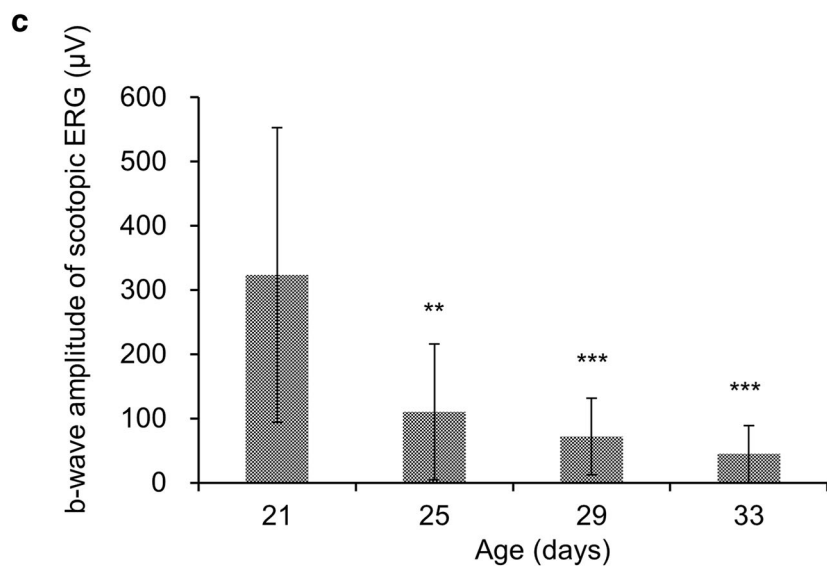
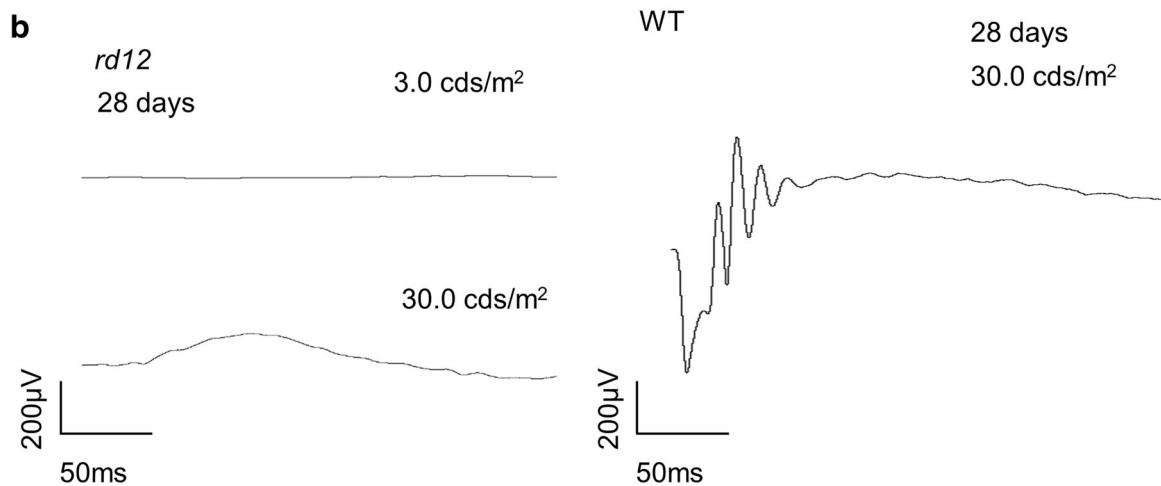
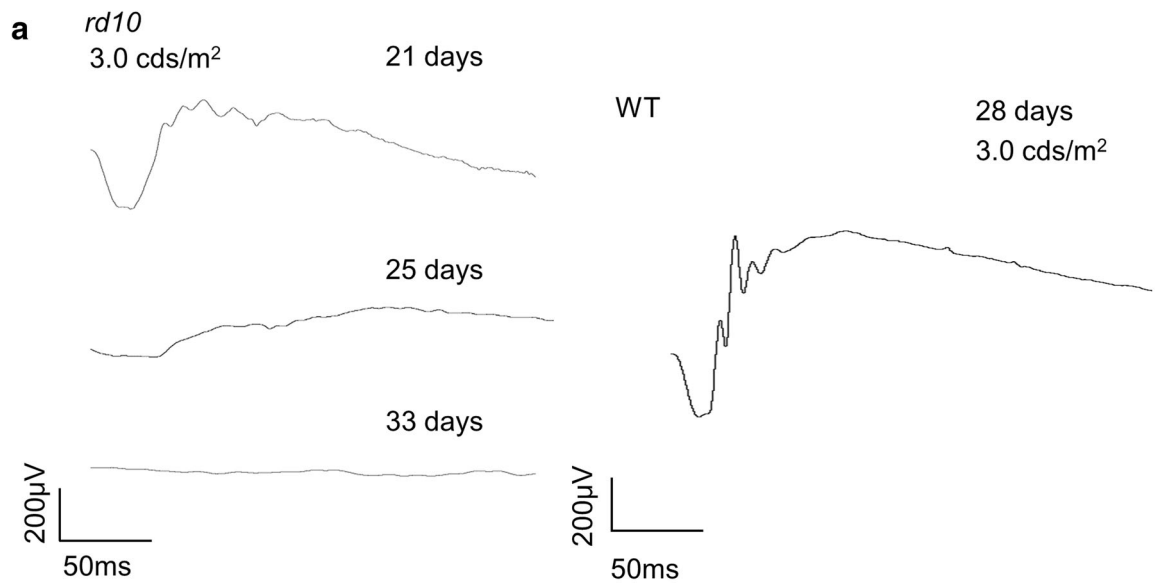
In this study, we assessed the histological and functional natural history of retinal degeneration in *rd10* and *rd12* mice, which are commonly used mouse models of retinitis pigmentosa and/or LCA. In *rd10* mice, photoreceptor degeneration, along with ONL and OS thinning, occurred between 21 and 25 days of age. This anatomical decline was also accompanied by a rapid reduction in visual function. In contrast, in *rd12* mice, visual function in the dark was not detectable at 1 month of age, as reported previously [17, 19], when the photoreceptors and ONL and OS thickness were better maintained.

Many studies have shown that the photoreceptor ellipsoid zone (also known as the IS/OS junction line) and the ELM line on SD-OCT images correlate well with retinal function [32–34]. We also found that vision declined with deterioration of the ELM line and ellipsoid zone visibility in *rd10* mice. In contrast, 1-month-old *rd12* mice did not have a detectable dark-adapted ERG, even though the ELM

Fig. 5 Scotopic electroretinogram (ERG) in *rd10*, *rd12*, and WT mice. **a** Left Scotopic ERGs (3.0 cds/m²) from an *rd10* mouse showing the median b-wave amplitude at 21, 25, and 33 days. At 21 days, a-wave, b-wave, and oscillatory potentials were detectable, but they were smaller than those in a 28-day-old WT mouse (right). At 25 days, a delayed, small b-wave was present, but the a-wave had almost disappeared. At 33 days, no ERG was detectable. **b** Left Scotopic ERGs (3.0, 30.0 cds/m²) from 28-day-old *rd12* mice showing median b-wave amplitude; a small b-wave was detectable at 30.0 cds/m² but not detectable at 3.0 cds/m². Right Scotopic ERG (30.0 cds/m²) from 28-day-old WT mouse. **c** Time-dependent changes in b-wave amplitude of scotopic ERG (3.0 cds/m²) in *rd10* mice. Error bars represent one standard deviation (SD). ** $P < 0.01$; *** $P < 0.001$ vs. scotopic ERG at 21 days, Bonferroni post hoc test

line and ellipsoid zone were visible or partially visible in most eyes until 13 months of age. These results imply that the status of neither the ellipsoid zone nor the ELM line is disrupted simultaneously with the ERG in *rd12* mice. Jacobson et al. [38] showed that LCA patients with *RPE65* mutations had relatively preserved retinal layer thickness despite their advanced visual loss. It may be that the difference in the discrepancies between morphology and visual function are dependent on visual cycle function in animal models and in human patients. The *rd10* mice have a missense mutation in *Pde6b* [15] which reduces the expression of beta-phosphodiesterase (PDE) in rod photoreceptors. Reduced levels of beta-PDE do not hinder the visual cycle and, therefore, live photoreceptors can respond to light in *rd10* mice. However, reduced levels of beta-PDE cause intracellular cGMP accumulation and, consequently, hyperexcitable photoreceptor cell death [15]. In *rd12* mice, functional RPE65 protein is not present in the RPE, causing a shortage of 11-*cis* retinal in the photoreceptors [17] and resulting in a dysfunctional visual cycle. Therefore, retinas of *rd12* mice at a relatively early stage, which look morphologically healthy (photoreceptors), are unable to respond to relatively weak light, unlike normally functioning retina. However, we did detect a small response in the photopic condition in 13-month-old *rd12* mice, possibly caused by reduced sensitivity of rods, similar to that reported by Seeliger et al. [39] for *Rpe65*^{-/-} mice. Even if *rd12* mice and LCA patients with *RPE65* mutations have poor visual function, relatively preserved retinal structures may provide us with a longer therapeutic time window.

Using SD-OCT images, we detected hyper-reflectivity of the layers corresponding to the photoreceptors in 21-day-old *rd10* mice. This result is in agreement with previous findings [26]. Because the hyper-reflectivity disappeared at later stages, we believe that hyper-reflectivity reflects an acute phase of degeneration. One possible explanation is that the hyper-reflectivity resulted from the disorganization of the outer retina that was observed on the electron microscopy images and HE-stained retinal



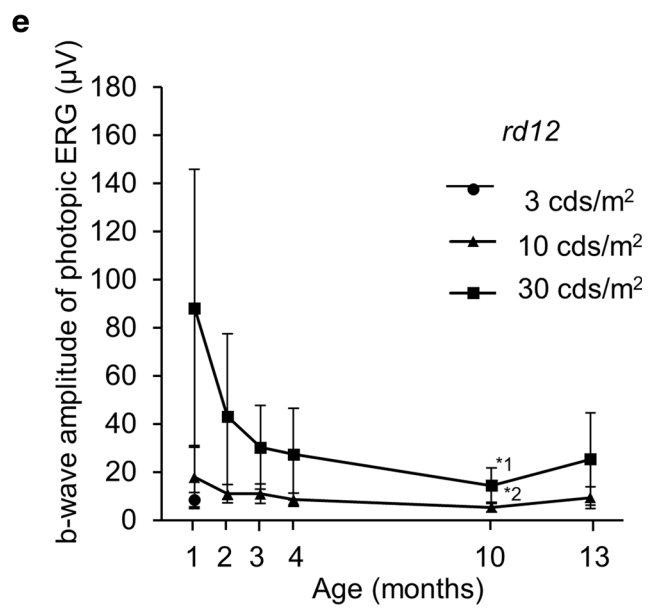
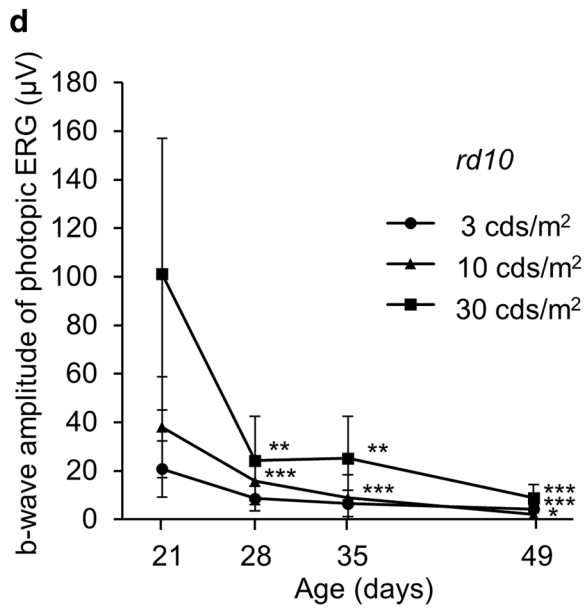
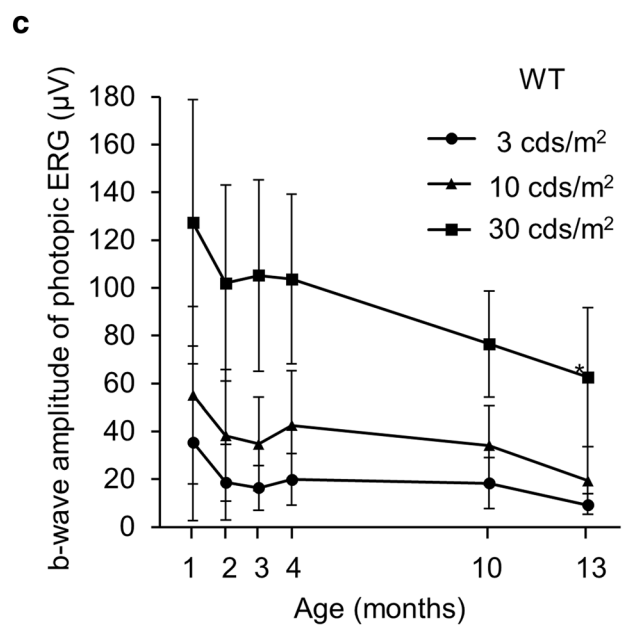
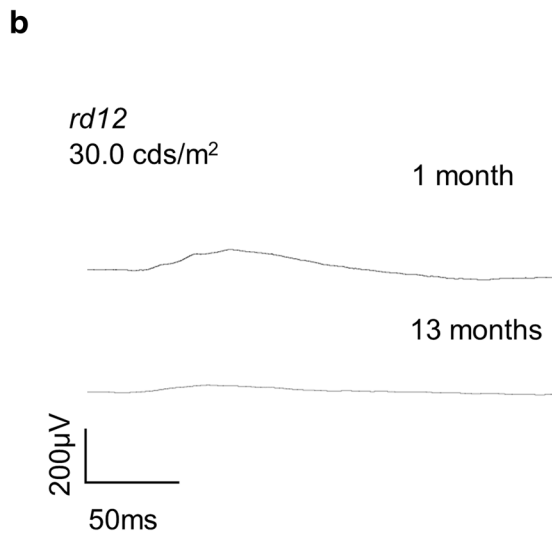
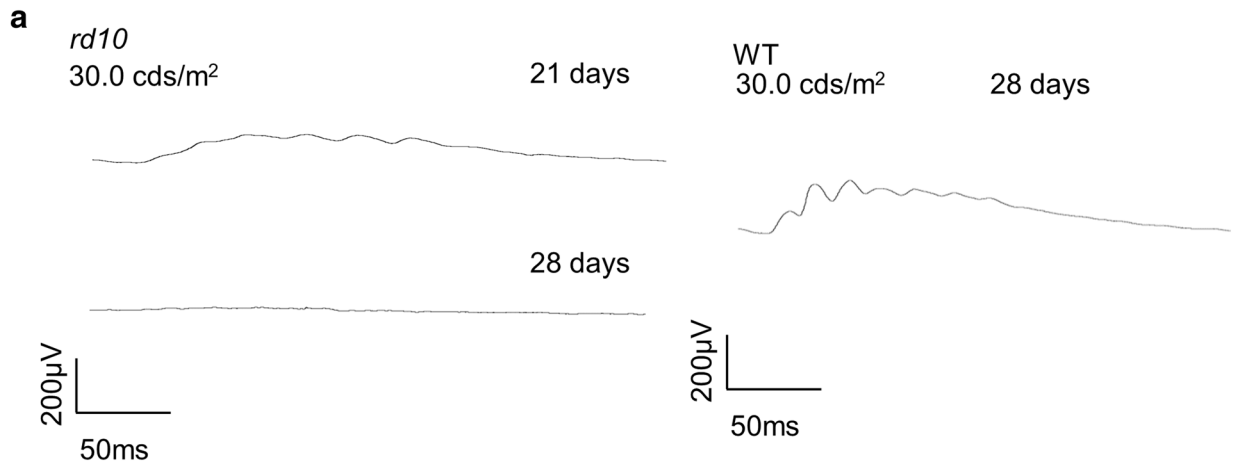


Fig. 6 Photopic electroretinogram (ERG) from *rd10*, *rd12*, and WT mice. **a** Left Photopic ERGs (30.0 cds/m²) from 21- and 28-day-old *rd10* mice showing median b-wave amplitude. At 21 days, a small and delayed b-wave and oscillatory potentials were detected, but the a-wave was almost undetectable. At 28 days, the photopic ERG was undetectable. **Right** Photopic ERG (30.0 cds/m²) from a 1-month-old WT mouse showing median b-wave amplitude. **b** Photopic ERG (30.0 cds/m²) from 1- and 13-month-old *rd12* mice showing median b-wave amplitude. The a-wave was undetectable at 1 month. A small b-wave was still detectable at 13 months. **c–e** The photopic ERG b-wave amplitude from WT (**c**), *rd10* (**d**) and *rd12* (**e**) mice recorded with 3.0, 10.0, and 30.0 cds/m² stimuli. Error bars represent one SD. **c** **P* < 0.05 vs. ERG at 4 months, Bonferroni post hoc test. **d** **P* < 0.05; ***P* < 0.01; ****P* < 0.001 vs. ERG at 21 days, Bonferroni post hoc test. **e** *1 *P* < 0.05 versus 3 months; *2 *P* < 0.05 vs. ERG at 4 months, Bonferroni post hoc test

sections. In *rd12* mice in an early disease stage (21 days of age), morphological degeneration was not observed, but a weak, focal hyper-reflectivity was detected exclusively in the ONL. At a later disease stage (13 months of age), the hyper-reflectivity was only detected in the OS layer. The hyper-reflectivity in the OS layer is thought to be caused by a slight OS disorganization, which we confirmed to be present by electron microscopy. Hyper-reflective foci in the ONL have been reported in human patients with retinitis pigmentosa [40]. Electron microscopy images of 7-month-old *rd12* and 21-day-old *rd10* mice revealed the presence of intracellular vacuoles at the innermost ONL; these vacuoles are considered to be autophagosomes. This is consistent with recent reports that autophagy may be related to photoreceptor cell death during retinal degeneration [41, 42]. It is these vacuoles which are believed to be the cause of ONL hyper-reflectivity.

Many eyes in the *rd10* mice developed a retinal detachment, which has also been reported previously [26]. OCT enabled us to noninvasively observe the retina, in vivo, in these mice, which in turn allowed us to distinguish between true retinal detachments and those mechanically created during histological analyses. As observed on our SD-OCT images, many eyes developed retinal detachments at approximately 25 days of age, the time-point at which the photoreceptor degeneration was progressing. Interestingly, the detachment seemed to disappear within a few days, appearing again in later disease stages. Inflammatory reactions have been observed in retinitis pigmentosa patients [43, 44] and in *rd10* mice [26, 45]. In retinitis pigmentosa patients, macular edema is a complication that may worsen visual acuity [46]. Although the cause of macular edema in retinitis pigmentosa patients is not clearly understood, breakdown of the blood–retinal barrier associated with chronic inflammation [47–50], as well as RPE dysfunction [51] and vitreous traction [52, 53], is believed to be a possible mechanism. On the other hand, macular edema tends to occur where the outer retinal

structure is relatively preserved [46, 53]. We suggest that possible inflammation and consequent effusion accumulation lead to macular edema in retinitis pigmentosa patients and exudative retinal detachment in *rd10* mice whose outer retinal structure substantially decreases during the early stages (Figs. 1b, 2b; Table 1). We also believe that the rapid disappearance of photoreceptors likely causes an impaired attachment between the retina and the retinal pigmented epithelium, making the retina susceptible to detachment in *rd10* mice.

In conclusion, we have elucidated the precise natural course of a hereditary retinal degeneration in *rd10* and *rd12* mice. Retinal thickness substantially decreased in *rd10* mice, but only moderately decreased in *rd12* mice. We further found that retinal thickness and retinal structure, including the ellipsoid zone and the ELM, were relatively preserved in *rd12* mice, even at 13 months of age, and kept deteriorating gradually until 19 months of age. In addition, the photopic ERG b-wave was still detectable at 13 months in *rd12* mice. The findings of this study will be useful in improving our understanding of disease progression mechanisms and in investigating new treatments that may improve prognosis of retinitis pigmentosa patients, in particular those with *PDE6B* or *RPE65* mutations.

Acknowledgments We thank Hitomi Suetsugu for technical assistance and the Center for Anatomical, Pathological, and Forensic Medical Research for preparation of the histological sections. This study was supported by grants from the Ministry of Education, Culture, Sports, Science, and Technology of Japan (Grand-in-Aid for Young Scientists No. 24791850 and for the Innovative Techno-Hub for Integrated Medical Bio-Imaging of the Project for Developing Innovation Systems No. 24249082). This study was also supported by grants from the Ministry of Health, Labour and Welfare of Japan and Japan Society for the Promotion of Science.

Conflicts of interest T. Hasegawa, none; H.O. Ikeda, Grant (the Astellas Foundation for Research on Metabolic Disorders, the Japan Foundation for Applied Enzymology, the Uehara Memorial Foundation, YOKOYAMA Foundation for Clinical Pharmacology, Mochida Memorial Foundation, Japan Intractable Diseases Research Foundation, Japan Research Foundation for Clinical Pharmacology); N. Nakano, none; Y. Muraoka, none; T. Tsuruyama, None; K. O. Furuta, none; H. Kohda, none; N. Yoshimura, grant (Nidek, Topcon, Canon, Novartis Japan, Bayer, Santen, Senju), honorary (Nidek, Canon, Novartis Japan, Bayer, Santen, Senju), and consultant fee (Nidek, Canon).

References

- Shintani K, Shechtman DL, Gurwood AS. Review and update: current treatment trends for patients with retinitis pigmentosa. *Optometry*. 2009;80:384–401.
- Ng TK, Fortino VR, Pelaez D, Cheung HS. Progress of mesenchymal stem cell therapy for neural and retinal diseases. *World J Stem Cells*. 2014;6:111–9.

3. Acland GM, Aguirre GD, Ray J, Zhang Q, Aleman TS, Cideciyan AV, et al. Gene therapy restores vision in a canine model of childhood blindness. *Nat Genet.* 2001;28:92–5.
4. Cai X, Conley SM, Naash MI. RPE65: role in the visual cycle, human retinal disease, and gene therapy. *Ophthalmic Genet.* 2009;30:57–62.
5. Sieving PA, Caruso RC, Tao W, Coleman HR, Thompson DJ, Fullmer KR, et al. Ciliary neurotrophic factor (CNTF) for human retinal degeneration: phase I trial of CNTF delivered by encapsulated cell intraocular implants. *Proc Natl Acad Sci USA.* 2006;103:3896–901.
6. Yang PB, Seiler MJ, Aramant RB, Yan F, Mahoney MJ, Kitzes LM, et al. Trophic factors GDNF and BDNF improve function of retinal sheet transplants. *Exp Eye Res.* 2010;91:727–38.
7. Yang Y, Mohand-Said S, Danan A, Simonutti M, Fontaine V, Clerin E, et al. Functional cone rescue by RdCVF protein in a dominant model of retinitis pigmentosa. *Mol Ther.* 2009;17:787–95.
8. Chizzolini M, Galan A, Milan E, Sebastiani A, Costagliola C, Parmeggiani F. Good epidemiologic practice in retinitis pigmentosa: from phenotyping to biobanking. *Curr Genomics.* 2011;12:260–6.
9. Hartong DT, Berson EL, Dryja TP. Retinitis pigmentosa. *Lancet.* 2006;368:1795–809.
10. Oishi M, Oishi A, Gotoh N, Ogino K, Higasa K, Iida K, et al. Comprehensive molecular diagnosis of a large cohort of Japanese retinitis pigmentosa and usher syndrome patients by next-generation sequencing. *Invest Ophthalmol Vis Sci.* 2014;55:7369–75.
11. den Hollander AI, Roepman R, Koenekoop RK, Cremers FP. Leber congenital amaurosis: genes, proteins and disease mechanisms. *Prog Retin Eye Res.* 2008;27:391–419.
12. Bainbridge JW, Smith AJ, Barker SS, Robbie S, Henderson R, Balagan K, et al. Effect of gene therapy on visual function in Leber's congenital amaurosis. *N Engl J Med.* 2008;358:2231–9.
13. Bennett J, Ashtari M, Wellman J, Marshall KA, Cyckowski LL, Chung DC, et al. AAV2 gene therapy readministration in three adults with congenital blindness. *Sci Transl Med.* 2012;4:120ra15.
14. Maguire AM, Simonelli F, Pierce EA, Pugh EN Jr, Mingozzi F, Bennicelli J, et al. Safety and efficacy of gene transfer for Leber's congenital amaurosis. *N Engl J Med.* 2008;358:2240–8.
15. Chang B, Hawes NL, Pardue MT, German AM, Hurd RE, Davisson MT, et al. Two mouse retinal degenerations caused by missense mutations in the beta-subunit of rod cGMP phosphodiesterase gene. *Vis Res.* 2007;47:624–33.
16. Rivas MA, Vecino E. Animal models and different therapies for treatment of retinitis pigmentosa. *Histol Histopathol.* 2009;24:1295–322.
17. Pang JJ, Chang B, Hawes NL, Hurd RE, Davisson MT, Li J, et al. Retinal degeneration 12 (rd12): a new, spontaneously arising mouse model for human Leber congenital amaurosis (LCA). *Mol Vis.* 2005;11:152–62.
18. Redmond TM, Yu S, Lee E, Bok D, Hamasaki D, Chen N, et al. Rpe65 is necessary for production of 11-*cis*-vitamin A in the retinal visual cycle. *Nat Genet.* 1998;20:344–51.
19. Zheng Q, Ren Y, Tzekov R, Zhang Y, Chen B, Hou J, et al. Differential proteomics and functional research following gene therapy in a mouse model of Leber congenital amaurosis. *PLoS ONE.* 2012;7:e44855.
20. Huang D, Swanson EA, Lin CP, Schuman JS, Stinson WG, Chang W, et al. Optical coherence tomography. *Science.* 1991;254:1178–81.
21. Jaffe GJ, Caprioli J. Optical coherence tomography to detect and manage retinal disease and glaucoma. *Am J Ophthalmol.* 2004;137:156–69.
22. Hangai M, Yamamoto M, Sakamoto A, Yoshimura N. Ultrahigh-resolution versus speckle noise-reduction in spectral-domain optical coherence tomography. *Opt Express.* 2009;17:4221–35.
23. Huber G, Beck SC, Grimm C, Sahaboglu-Tekgoz A, Paquet-Durand F, Wenzel A, et al. Spectral domain optical coherence tomography in mouse models of retinal degeneration. *Invest Ophthalmol Vis Sci.* 2009;50:5888–95.
24. Kim KH, Puoris'haag M, Maguluri GN, Umino Y, Cusato K, Barlow RB, et al. Monitoring mouse retinal degeneration with high-resolution spectral-domain optical coherence tomography. *J Vis.* 2008;8:17.1–17.11.
25. Pang JJ, Dai X, Boye SE, Barone I, Boye SL, Mao S, et al. Long-term retinal function and structure rescue using capsid mutant AAV8 vector in the rd10 mouse, a model of recessive retinitis pigmentosa. *Mol Ther.* 2011;19:234–42.
26. Pennesi ME, Michaels KV, Magee SS, Maricle A, Davin SP, Garg AK, et al. Long-term characterization of retinal degeneration in rd1 and rd10 mice using spectral domain optical coherence tomography. *Invest Ophthalmol Vis Sci.* 2012;53:4644–56.
27. Ruggeri M, Wehbe H, Jiao S, Gregori G, Jockovich ME, Hackam A, et al. In vivo three-dimensional high-resolution imaging of rodent retina with spectral-domain optical coherence tomography. *Invest Ophthalmol Vis Sci.* 2007;48:1808–14.
28. Wang R, Jiang C, Ma J, Young MJ. Monitoring morphological changes in the retina of rhodopsin-/- mice with spectral domain optical coherence tomography. *Invest Ophthalmol Vis Sci.* 2012;53:3967–72.
29. Nakano N, Ikeda HO, Hangai M, Muraoka Y, Toda Y, Kakizuka A, et al. Longitudinal and simultaneous imaging of retinal ganglion cells and inner retinal layers in a mouse model of glaucoma induced by *N*-methyl-D-aspartate. *Invest Ophthalmol Vis Sci.* 2011;52:8754–62.
30. Muraoka Y, Ikeda HO, Nakano N, Hangai M, Toda Y, Okamoto-Furuta K, et al. Real-time imaging of rabbit retina with retinal degeneration by using spectral-domain optical coherence tomography. *PLoS ONE.* 2012;7:e36135.
31. Marmor MF, Fulton AB, Holder GE, Miyake Y, Brigell M, Bach M. ISCEV standard for full-field clinical electroretinography (2008 update). *Doc Ophthalmol.* 2009;118:69–77.
32. Staurengi G, Sadda S, Chakravarthy U, Spaide RF. Proposed lexicon for anatomic landmarks in normal posterior segment spectral-domain optical coherence tomography: the IN*OCT consensus. *Ophthalmology.* 2014;121:1572–8.
33. Wong IY, Iu LP, Koizumi H, Lai WW. The inner segment/outer segment junction: what have we learnt so far? *Curr Opin Ophthalmol.* 2012;23:210–8.
34. Oishi A, Hata M, Shimozone M, Mandai M, Nishida A, Kurimoto Y. The significance of external limiting membrane status for visual acuity in age-related macular degeneration. *Am J Ophthalmol.* 2010;150(27–32):e1.
35. Breton ME, Schueller AW, Lamb TD, Pugh EN Jr. Analysis of ERG a-wave amplification and kinetics in terms of the G-protein cascade of phototransduction. *Invest Ophthalmol Vis Sci.* 1994;35:295–309.
36. Hood DC, Birch DG. Beta wave of the scotopic (rod) electroretinogram as a measure of the activity of human on-bipolar cells. *J Opt Soc Am A Opt Image Sci Vis.* 1996;13:623–33.
37. Korol S, Leuenberger PM, Englert U, Babel J. In vivo effects of glycine on retinal ultrastructure and averaged electroretinogram. *Brain Res.* 1975;97:235–51.
38. Jacobson SG, Aleman TS, Cideciyan AV, Sumaroka A, Schwartz SB, Windsor EA, et al. Identifying photoreceptors in blind eyes caused by RPE65 mutations: prerequisite for human gene therapy success. *Proc Natl Acad Sci USA.* 2005;102:6177–82.
39. Seeliger MW, Grimm C, Stahlberg F, Friedburg C, Jaissle G, Zrenner E, et al. New views on RPE65 deficiency: the rod system is the source of vision in a mouse model of Leber congenital amaurosis. *Nat Genet.* 2001;29:70–4.
40. Kuroda M, Hiramami Y, Hata M, Mandai M, Takahashi M, Kurimoto Y. Intraretinal hyperreflective foci on spectral-domain

- optical coherence tomographic images of patients with retinitis pigmentosa. *Clin Ophthalmol*. 2014;8:435–40.
41. Bo Q, Ma S, Han Q, Wang FE, Li X, Zhang Y. Role of autophagy in photoreceptor cell survival and death. *Crit Rev Eukaryot Gene Expr*. 2015;25:23–32.
 42. Sancho-Pelluz J, Arango-Gonzalez B, Kustermann S, Romero FJ, van Veen T, Zrenner E, et al. Photoreceptor cell death mechanisms in inherited retinal degeneration. *Mol Neurobiol*. 2008;38:253–69.
 43. Newsome DA, Michels RG. Detection of lymphocytes in the vitreous gel of patients with retinitis pigmentosa. *Am J Ophthalmol*. 1988;105:596–602.
 44. Yoshida N, Ikeda Y, Notomi S, Ishikawa K, Murakami Y, Hisatomi T, et al. Clinical evidence of sustained chronic inflammatory reaction in retinitis pigmentosa. *Ophthalmology*. 2013;120:100–5.
 45. Yoshida N, Ikeda Y, Notomi S, Ishikawa K, Murakami Y, Hisatomi T, et al. Laboratory evidence of sustained chronic inflammatory reaction in retinitis pigmentosa. *Ophthalmology*. 2013;120:e5–12.
 46. Sahel J, Bonnel S, Mrejen S, Paques M. Retinitis pigmentosa and other dystrophies. *Dev Ophthalmol*. 2010;47:160–7.
 47. Cunha-Vaz JG, Travassos A. Breakdown of the blood–retinal barriers and cystoid macular edema. *Surv Ophthalmol*. 1984;28:485–92.
 48. Fishman GA, Cunha-Vaz J, Salzano T. Vitreous fluorophotometry in patients with retinitis pigmentosa. *Arch Ophthalmol*. 1981;99:1202–7.
 49. Kuchle M, Nguyen NX, Martus P, Freissler K, Schalnus R. Aqueous flare in retinitis pigmentosa. *Graefes Arch Clin Exp Ophthalmol*. 1998;236:426–33.
 50. Vinos SA, Kuchle M, Derevjanik NL, Henderer JD, Mahlow J, Green WR, et al. Blood-retinal barrier breakdown in retinitis pigmentosa: light and electron microscopic immunolocalization. *Histol Histopathol*. 1995;10:913–23.
 51. Cox SN, Hay E, Bird AC. Treatment of chronic macular edema with acetazolamide. *Arch Ophthalmol*. 1988;106:1190–5.
 52. Fishman GA, Fishman M, Maggiano J. Macular lesions associated with retinitis pigmentosa. *Arch Ophthalmol*. 1977;95:798–803.
 53. Makiyama Y, Oishi A, Otani A, Ogino K, Nakagawa S, Kurimoto M, et al. Prevalence and spatial distribution of cystoid spaces in retinitis pigmentosa: investigation with spectral domain optical coherence tomography. *Retina*. 2014;34:981–8.